Available online at www.sciencedirect.com
SCIENCE DIRECT
Journal of Catalysis 234 (2005) 119–130
JOURNAL OF CATALYSIS
www.elsevier.com/locate/jcat

Application of calcined Mg–Al hydrotalcites for Michael additions: an investigation of catalytic activity and acid–base properties

Hillary A. Prescott [a], Zhi-Jian Li [a], Erhard Kemnitz [a,*], Annette Trunschke [b], Jens Deutsch [b], Heiner Lieske [b], Aline Auroux [c]

[a] *Humboldt-Universität zu Berlin, Institut für Chemie, Brook-Taylor-Strasse 2, D-12489 Berlin, Germany*
[b] *Institut für Angewandte Chemie Berlin-Adlershof, Richard-Willstätter-Strasse 12, D-12489 Berlin, Germany*
[c] *Institut de Recherches sur la Catalyse, UPR CNRS 5401, 2, Av. A. Einstein, 69626 Villeurbanne cedex, France*

Received 11 April 2005; revised 3 June 2005; accepted 6 June 2005

Available online 14 July 2005

Abstract

Mg–Al hydrotalcite catalysts with different Mg/Al molar ratios (0.6, 1.4, 2.2, 3.0) were calcined and tested in liquid-phase Michael additions at room temperature. The catalysts and pure oxides (MgO and Al_2O_3) were characterized by XRD, XPS, N_2 adsorption experiments, ^{27}Al MAS NMR, and TG-DTA. The acid–base properties of the samples were investigated by (a) FTIR spectroscopy after pyridine and CO_2 adsorption and (b) microcalorimetry with CO_2 and benzoic acid. Both acid sites (Lewis) and base sites (Lewis and Brønsted) are present on the surface of calcined hydrotalcites. The calcined hydrotalcites (CHT) catalyzed the Michael additions of CH-acid compounds to methyl vinyl ketone to give high product yields with 100% selectivity; the Al-rich sample exhibited the highest activity.

Keywords: Hydrotalcite; Mg–Al mixed oxide; Acid–base properties; Solid base catalyst; Michael addition

1. Introduction

Base-catalyzed C–C bond coupling reactions, such as the Michael addition, are used for the production of pharmaceuticals and fine chemicals. Soluble bases, such as alkali hydroxides, alkali alcoholates, or amines, conventionally catalyze these liquid-phase reactions, yet environmental and economical concerns are driving the replacement of soluble bases with solid bases [1,2].

Solid base catalyst systems, such as $Ba(OH)_2$ [3], MgO [4,5], KF/Al_2O_3 [6], and $Na/NaOH/Al_2O_3$ [7], have been used in various Michael additions. A highly active, selective base catalyst for the Michael addition of 2-methylcyclohexane-1,3-dione to methyl vinyl ketone was potassium-modified ZrO_2, yet the leaching of its potassium species made it unsuitable as a heterogeneous catalyst [8]. Recently, Choudary et al. [9] found that a rehydrated Mg–Al hydrotalcite was an efficient, very selective catalyst for Michael additions; the untreated and calcined hydrotalcites were inactive.

Hydrotalcites are commercially available and cheap solid bases; hydrotalcites and calcined hydrotalcites (normally referred to as mixed oxides) are highly active, selective catalysts and play an important role in many base-catalyzed reactions, such as Claisen–Schmidt condensations [10] and Knoevenagel condensations [11]. The synthesis, the textural and acid–base properties, and the catalytic application of hydrotalcites and calcined hydrotalcites were reviewed in [12–15]. Their surface base sites were characterized by temperature-programmed desorption (TPD) after adsorption of CO_2 [16,17], FTIR spectroscopy with CO_2 [18–20], and gas-phase microcalorimetry (with CO_2 and SO_2) [18,21–23]. In addition to base sites, acid sites or acid–base pairs on these materials also influence the catalytic performance. Acid–base sites on mixed oxides are highly active sites for

* Corresponding author. Tel: +49-30-2093-7277.
E-mail address: erhard.kemnitz@chemie.hu-berlin.de (E. Kemnitz).

0021-9517/$ – see front matter
doi:10.1016/j.jcat.2005.06.004

many reactions: Meerwein–Ponndorf–Verley reactions [24], cycloadditions of carbon dioxide to epoxides [25], and aldol condensations to form nonenal [26]. Acid–base properties of Mg–Al mixed oxides are governed by the Mg/Al molar ratio [17–19], calcination temperature [21], and preparation condition [16,20,27,28]. Although the acid–base properties are generally known to be important for catalytic activity and selectivity, the intricate relationship between catalytic behavior in Michael additions, acid–base properties, and the composition of hydrotalcite and calcined hydrotalcites is still poorly understood.

Thus, the aim of this work was (a) to find an efficient, selective catalyst that is easily acquired and cheap and whose properties are reproducible and reliable for large-scale technical Michael additions and (b) to study the influence of its acid–base properties and chemical composition on the catalytic performance of the calcined hydrotalcites. The Michael addition of 1,3-diones with different pK_a values to methyl vinyl ketone was examined on calcined commercial Mg–Al hydrotalcites including an Al-rich sample. Acid–base properties of the catalysts were investigated by gaseous probe molecules with FTIR spectroscopy and microcalorimetry. Microcalorimetric measurements were carried out with benzoic acid to study catalyst basicity under liquid-phase conditions similar to those of the liquid-phase test reactions.

2. Experimental

2.1. Catalyst preparation

Hydrotalcites (Pural MG 30, 50, 61, 70 from SASOL Germany GmbH) [29] were calcined at 550 °C in air for 3 h. Al_2O_3 was obtained by calcination of AlO(OH) (Pural SB, SASOL Germany GmbH) [29] under the same conditions. Calcination of dried $Mg(OH)_2$ at 600 °C in air for 4 h produced MgO. The hydroxide was precipitated from $Mg(NO_3)_2$ with KOH and dried at 110 °C. The samples are denoted in the following way: HT0.6 or CHT0.6 signifies the sample with a bulk Mg/Al molar ratio of 0.6; the C in the sample code indicates that the sample has been calcined (Table 1).

2.2. Catalyst characterization

2.2.1. XRD, N_2 adsorption experiments, ICP-OES, and XPS

X-ray powder diffraction (XRD) was performed with Cu-K_α radiation ($\lambda = 1.5418$ Å, 40 kV, and 35 mA; RD 7, Rich. Seifert GmbH & Co. KG, Freiberg, Germany) over the 2θ range from 5° to 65° or 90°. One sample, HT0.6, was calcined further at 700 °C to clearly interpret the pattern of amorphous CHT0.6 (calcination temperature: 550 °C). Nitrogen adsorption experiments were carried out at 77 K with a surface area analyzer (Micromeritics; ASAP2010); samples were degassed at 100 °C until the static vacuum was constant. The specific surface area was calculated by the BET method. Carbon contents of hydrotalcites were determined by elemental analysis (Leco CHNS-932 element analyzer). Bulk and surface Mg/Al molar ratios were determined by ion-coupled plasma optical emission spectroscopy (ICP-OES) (Unicam 701) and X-ray photoelectron spectroscopy (XPS) (VG Escalab 220 iXL spectrometer with a Mg-K_α source and a monochromated Al-K_α source), respectively.

2.2.2. ^{27}Al MAS NMR

We performed ^{27}Al MAS NMR experiments by accumulating 64 scans on a Bruker Avance 400 spectrometer at a resonance frequency of 104.3 MHz with an excitation of $\pi/6$ pulses and a repetition time of 5 s. A commercial Bruker 4-mm probe was used to perform the MAS experiments with a spinning rate of 10 kHz. The reference for the chemical shifts was an aqueous 1 M solution of aluminum chloride.

2.2.3. Thermal analysis

Thermogravimetry (TG) and differential thermal analysis (DTA) were performed with a Netzsch STA409C system equipped with a skimmer-coupled mass spectrometer in air at a heating rate of 10 °C/min from room temperature to 700 °C (reference: Al_2O_3).

2.2.4. FTIR spectroscopy

FTIR measurements were carried out on self-supporting wafers (10–40 mg) in a transmission IR quartz cell with CaF_2 window. The samples were pretreated at 550 °C in flowing synthetic air for 1 h and then under vacuum for 30 min. The adsorption of pyridine (Merck; freshly distilled and stored over zeolite A) was then performed at 40 °C with 0–15 mbar pyridine and subsequent evacuation for 10 min to remove physisorbed pyridine. An IR spectrum was measured every 50 °C during temperature-programmed desorption (TPD) from 100 to 300 °C (heating rate of 10 °C/min) after evacuation for 10 min. In the case of CO_2 adsorption (Messer Griesheim; 99.995 vol%), the samples were pretreated under vacuum at 400 °C for 1 h. The measurement conditions were identical to those used after pyridine adsorption, except for the TPD evacuation time of 10 min, which was lengthened to 30 min. IR spectra (64 scans, resolution of 2 cm^{-1}) were recorded on a Digilab FTS-60A spectrometer. The background spectrum was measured before adsorption; spectra were normalized by the wafer weight (10 mg).

2.2.5. Microcalorimetric measurements

2.2.5.1. Gas-phase experiments with CO_2 Microcalorimetric data were collected with a heat flow Tian–Calvet-type calorimeter (C 80, Setaram) connected to a volumetric line with an online injection system for pulsing reactive gases. CO_2 (> 99.9%) was pulsed from a storage vessel. After each pulse, the equilibrium pressure was measured with a differential pressure gauge (Barocel, Datametrics). The

calorimetric and volumetric data (pressure, adsorbed volume, heats of adsorption, differential and integral enthalpies) were stored and analyzed with a microcomputer. The sample (70–100 mg) was pretreated under vacuum overnight at 400 °C. The first adsorption cycle was complete after a final equilibrium pressure of 0.6 Torr was reached at 40 °C; the system was then evacuated to remove the physisorbed CO_2, and a second adsorption cycle was performed. For the samples measured here, the level of irreversible adsorption was almost constant above 0.2 Torr. Thus, the amount of totally adsorbed (chemisorbed and physisorbed) CO_2 was determined from the first isotherm; the quantity of irreversibly adsorbed (chemisorbed) CO_2 was determined by the difference between the isotherms of the first and second adsorption cycles.

2.2.5.2. Liquid-phase experiments with benzoic acid Liquid-phase experiments were performed on a Titrys calorimeter (Setaram) with a stirring system. The samples (about 200 mg) were pretreated under vacuum overnight at 400 °C and then transferred to the calorimetric cell, which contained toluene (1.5 ml). The reference cell contained the same amount of toluene before injection. The experiments were carried out at 70 °C except for that with MgO, which was done at 40 °C. A solution of benzoic acid in toluene (0.0307 mol/l) was injected stepwise (0.2 ml, injection rate: 0.05 ml/min) every 2 h. The amount of unreacted benzoic acid was measured by UV spectrofluorimetry.

2.2.6. Catalytic experiments

Michael addition test reactions were carried out in a closed 50-ml round-bottomed flask at room temperature.

2.2.6.1. Michael addition of 2-methylcyclohexane-1,3-dione The solid, partially insoluble dione, 2-methylcyclohexane-1,3-dione (15 mmol; Acros, 98%), recrystallized from methanol before use, was suspended in a mixture of methyl vinyl ketone (22.5 mmol; Aldrich, 99%) and the solvent, methanol (10 ml; Aldrich, 99%). The mixture was stirred for 30 min to saturate the liquid phase with the CH-acid; the saturation concentration of the 1,3-dione was 0.15 M (10% of its total amount in the mixture) after 30 min. The catalyst (0.225 g HT or the respective amount of CHT after calcination of 0.225 g HT; see Table 1) was then added.

2.2.6.2. Michael addition of 2-acetylcyclopentanone and 2-acetylcyclohexanone The liquid diones, 2-acetylcyclopentanone (15 mmol; Aldrich, 98%) and 2-acetylcyclohexanone (15 mmol; Aldrich, 97%), were added to methyl vinyl ketone (15.0 mmol) in 10 ml methanol. The catalyst (0.225 g) was then added to the clear solution.

2.2.6.3. Sampling The internal NMR standard, dimethyl phthalate (3.75 mmol; Acros, 99%), was added to the reaction mixtures described above for a quantitative determination of product yields. To monitor the product formation, samples (about 0.3 ml) were taken periodically and centrifuged; the separated clear solutions were then concentrated on a rotary evaporator to remove solvent and unreacted methyl vinyl ketone.

2.2.6.4. NMR analysis of the catalytic yield Yields of the target product based on the 1,3-dione were quantitatively determined by ^{1}H NMR spectroscopy (solvent: DMSO-d_6 or $CDCl_3$), with the use of the integrals of the CH_3 signals of the internal standard, dimethyl phthalate (3.83 ppm in DMSO-d_6 and 3.88 ppm in $CDCl_3$) and those of the following Michael adducts: (a) 2-(3-oxo-butyl)-2-methylcyclohexane-1,3-dione (1.11 and 2.04 ppm, DMSO-d_6); (b) 2-acetyl-2-(3-oxo-butyl)-cyclopentanone (2.14 and 2.09 ppm, $CDCl_3$); and (c) 2-acetyl-2-(3-oxo-butyl)-cyclohexanone (2.08 ppm, $CDCl_3$; only one CH_3 signal was used, because the other overlapped with that of the 1,3-dione).

2.2.6.5. Experiments on the type of catalysis These experiments were carried out in the reactions with 2-methylcyclohexane-1,3-dione and 2-acetylcyclohexanone for CHT0.6 in methanol and with 2-acetylcyclopentanone in the absence of the solvent, methanol. The catalyst was separated by centrifugation from the reaction mixture after a given amount of time: 6 h for the reaction with 2-methylcyclohexane-1,3-dione and 4 h for the reactions with 2-acetylcyclopentanone and 2-acetylcyclohexanone. The product yield was then monitored with NMR after 20 h. The cation content in the reaction solution was determined with EDTA titration (0.01 M). In the case of Al^{3+}, EDTA (5 ml) was added to the solution and then the solution was back-titrated with $ZnSO_4$ (0.01 M) at pH 5.0 (sodium acetate buffer). The Mg content was determined by direct titration with EDTA at pH 10.0 (ammonium buffer), and subtraction of the Al content was determined.

3. Results and discussion

3.1. Physical properties of the catalysts

The physical properties of the HT and CHT samples and the reference materials, MgO and Al_2O_3, are listed in Table 1. All of the HT samples except for Al-rich HT0.6 have low specific surface areas and high average pore diameters. The high surface area and low pore diameter of HT0.6 may be due to a separate, minor phase of boehmit in this sample (Fig. 1A: d for XRD pattern). Sample calcination increases the specific surface area independently of composition and decreases the average pore diameter (exception: CHT0.6).

The ICP-OES results verified the identical Mg/Al molar ratios of the corresponding HT and CHT samples, yet the surface Mg/Al molar ratios (XPS measurements) of the CHT samples deviate from the bulk ratios. The surface Mg/Al ratio for CHT0.6 is slightly higher than the bulk ratio, whereas the bulk and surface ratios of CHT1.4

Table 1
Properties of hydrotalcites (HT), calcined hydrotalcites (CHT), MgO, and Al_2O_3

Sample	Theor. ratio Al/(Al + Mg)	Mg/Al molar ratio			S_{BET} (m^2/g)	V_p (cm^3/g)	d_p[a] (Å)	C[b] (wt%)	Weight loss[c] (wt%)
		Theor.	Bulk (ICP)	Surface (XPC)					
HT0.6 (MG30)	0.67	0.5	0.6	n.d.	163	0.32	76	1.42	31
HT1.4 (MG50)	0.44	1.25	1.4	n.d.	13	0.05	167	1.19	36
HT2.2 (MG61)	0.33	2.0	2.2	n.d.	15	0.05	128	2.42	42
HT3.0 (MG70)	0.25	3.0	3.0	n.d.	20	0.10	205	2.27	44
CHT0.6	0.67	0.5	0.6	0.8	257	0.52	81	–	–
CHT1.4	0.44	1.25	1.4	1.4	201	0.23	45	–	–
CHT2.2	0.33	2.0	2.2	2.0	114	0.13	46	–	–
CHT3.0	0.25	3.0	3.0	2.0	203	0.22	52	–	–
MgO	–	–	–	–	75	0.96	258	–	–
Al_2O_3	–	–	–	–	234	0.54	45	–	–

[a] Average pore diameter.
[b] Carbon content.
[c] Based on the weight lost during calcination in air at 550 °C.

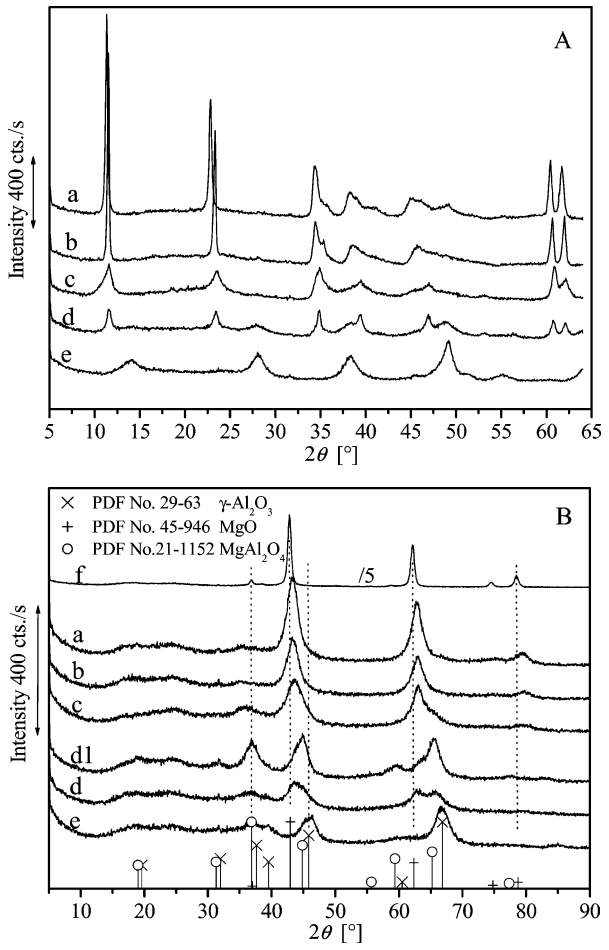

Fig. 1. XRD patterns of hydrotalcites (A), hydrotalcites calcined at 550 °C (B) with Mg/Al molar ratios of 3.0 (a), 2.2 (b), 1.4 (c), and 0.6 (d), MgO after calcination at 600 °C (intensity divided by a factor of 5, B: f), and the Al oxide before (boehmit in A: e) and after calcination (γ-Al_2O_3 in B: e). HT0.6 was calcined further at 700 °C (B: d1).

are identical. The surface of CHT2.2 and CHT3.0 are Al-enriched. In [16], Al-enriched surfaces were also found with XPS (Mg/Al = 1.5 and 2.4) for calcined Mg–Al hydrotalcites with Mg/Al molar ratios of 1.87 and 4.57, respectively.

The XRD patterns of the HT samples show a hydrotalcite-like structure similar to that presented in [27,28,30,31], whose crystallinity increases with Mg content (Fig. 1A: a–d). Additional weak peaks for boehmite are seen at 28° and 49° in the HT0.6 pattern (Fig. 1A: d, cf. Fig. 1A: e for Pural SB, AlO(OH), PDF No. 49-133) [29]. Calcination of the HT samples results in the destruction of the hydrotalcite-like structure and the formation of a periclase MgO (PDF no. 45-946, Fig. 1B: a–c), which is also found for pure MgO (Fig. 1B: f). Peaks for the periclase structure in CHT0.6 (Fig. 1B: d) were broad and low in intensity. The MgO peaks (at about 43° and 63°) of the CHT samples have higher 2θ values than those of pure MgO; this is caused by the incorporation of smaller Al^{3+} cations into the bulk lattice of the CHT samples [25,30–32]. The MgO peaks shift from higher to lower 2θ values as the Mg/Al ratio increases; thus, the amount of Al^{3+} cations incorporated decreases accordingly. These results agree with the XPS results. The AlO(OH) reference material forms γ-Al_2O_3 after calcination (PDF no. 29-63, Fig. 1B: e). Weak, broad peaks for $MgAl_2O_4$ (35°, PDF no. 21-1152) and γ-Al_2O_3 (66°) are observed in the patterns of CHT0.6 and CHT1.4. The spinel phase is formed to a higher degree after calcination of CHT0.6 at 700 °C (Fig. 1B: d1).

The ^{27}Al MAS NMR spectra of γ-Al_2O_3 and CHT samples (Fig. 2) have two broad signals at about 5 ppm for Al octahedra (Al_O) and 64 ppm for tetrahedrally coordinated aluminum cations (Al_T) [16,19,21,30,32]. The identical signal shapes of γ-Al_2O_3 and CHT0.6, particularly that of the 64-ppm signal, suggest similar Al environments. The low-field shift of the 5-ppm signal with increasing Mg/Al ratio indicates an increased number of Mg–O–Al_O linkages [19,21]. An absence of signal splitting [21] reflects indistinct Al coordination sites. The relatively narrow signal (at 5 ppm) of CHT1.4 could be attributed to more ordered AlO_6 octahedra and related to the sample homogeneity confirmed by ICP-OES and XPS.

The Al_T/Al_O ratio calculated from the integrated signals for Al_2O_3 is 0.38 and close to that reported in [16]. The

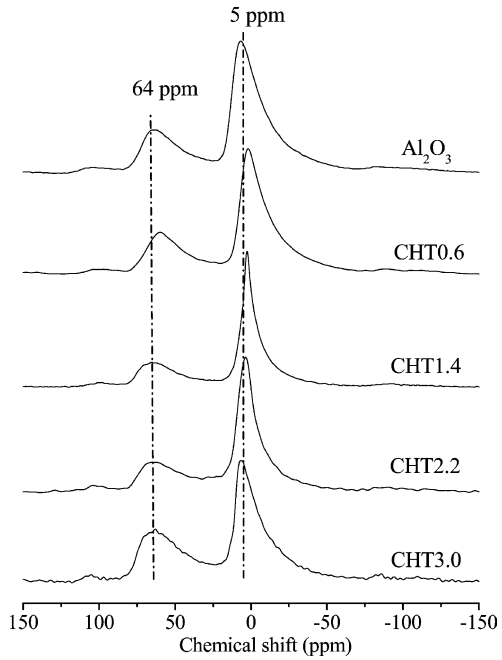

Fig. 2. ^{27}Al MAS NMR spectra of Al_2O_3 and the calcined hydrotalcites.

CHT samples have identical Al_T/Al_O ratios (0.38), except for that of CHT3.0 (0.59). This indicates that Al_T cations dominate in CHT3.0, possibly by the formation of inverse spinel-like domains: Mg–O–Al_T [19]. AlO_4 tetrahedra are generally formed during calcination [30,33]; the Al_T/Al_O ratio can also be influenced by the preparation method [16] and Al content [16,19]. The CHT samples were all calcined under the same conditions; thus, the higher Al_T/Al_O ratio in CHT3.0 can only result from the strong difference in bulk and surface Al contents not observed in the other samples. An increase in the Al_T/Al_O ratio with the Al *surface* concentration has been suggested before [16].

In the TG-DTA curves of HT0.6 and HT3.0 (Figs. 3a and 3b), gradual weight loss is observed from about 60 °C to approximately 600 °C, with two main endothermic effects at about 250 °C and 416 (432) °C. The first large endothermic effect at about 250 °C involves interlayer water loss ($m/z =$ 18) [27,34]; the second endothermic effect, at 432 °C, corresponds to the loss of OH^- groups and the decomposition of CO_3^{2-} in the brucite-like layers ($m/z = 44$) [27,34]. The total weight loss observed for HT0.6 and HT3.0 (ca. 33.5 and 42.5%, respectively) is similar to that calculated from weights taken before and after calcination (Table 1).

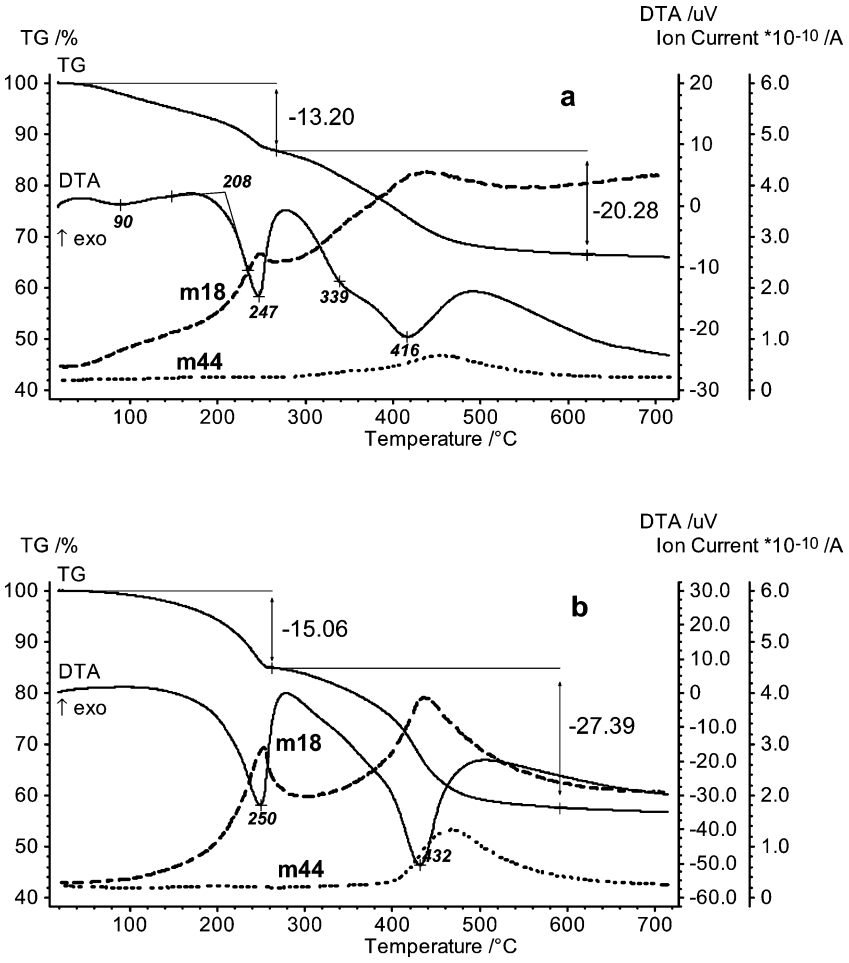

Fig. 3. TG-DTA profiles of hydrotalcites with the Mg/Al molar ratios: 0.6 (a) and 3.0 (b).

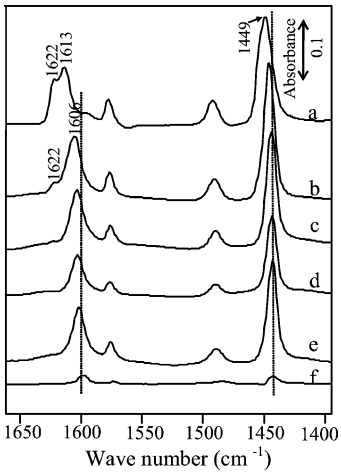

Fig. 4. Acid properties: pyridine adsorption on Al_2O_3 (a), the calcined hydrotalcites with Mg/Al molar ratios of 0.6 (b), 1.4 (c), 2.2 (d), and 3.0 (e), and MgO (f). Spectra were measured after adsorption and evacuation at 40 °C.

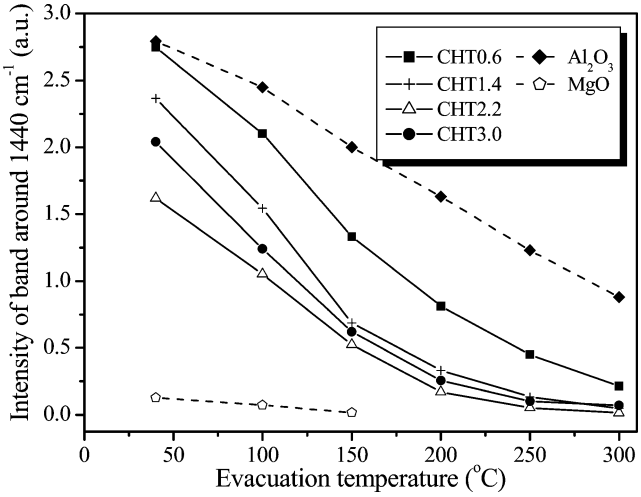

Fig. 5. Acid properties: temperature programmed desorption of pyridine. Effect of the evacuation temperature on the intensity of the band of adsorbed pyridine around 1440 cm^{-1}.

3.2. Acid–base properties of the catalysts

3.2.1. FTIR studies

3.2.1.1. Pyridine adsorption The spectra measured after pyridine adsorption at 40 °C on Al_2O_3, MgO, and the CHT samples are shown in Fig. 4. Stretching vibrations of pyridine molecules coordinatively bonded to Lewis acid sites are between 1630 and 1600 cm^{-1} (ν_{8a} mode) and 1450 and 1440 cm^{-1} (ν_{19b} mode). Brønsted acid sites (bands at 1640 and 1540 cm^{-1}) [35–37] were not found on any of the samples. Weak bands at 1600 and 1440 cm^{-1} for the negligible Lewis acidity of MgO (Fig. 4f) correspond to coordinatively unsaturated Mg^{2+} cations [36]. With increasing Al content, the ν_{8a} band shifts to higher wave numbers from 1601 cm^{-1} (CHT3.0, Fig. 4e) to 1613 cm^{-1} Al_2O_3 (Fig. 4a), corresponding to an increase in acid site strength. The band at 1613 cm^{-1} on Al_2O_3 can be attributed to pyridine bonded to a pair of coordinatively unsaturated Al^{3+} ions in octahedral (Al_O) and tetrahedral (Al_T) coordination [38–41]. An additional band at 1622 cm^{-1} (Fig. 4a) can be ascribed to pyridine strongly adsorbed on coordinatively unsaturated Al^{3+} ions in a tetrahedral environment (Al_T) [38–41]. A similar band of much lower intensity was observed for the CHT0.6 sample (Fig. 4b), which was possibly due to the presence of boehmite. The total amount of absorbed pyridine was estimated by integration of the band (ν_{19b} mode) around 1440 cm^{-1}. The value calculated after evacuation at different temperatures is plotted against the evacuation temperature in Fig. 5. The total number of Lewis acid sites is highest for Al_2O_3 and CHT0.6 and then decreases in the following order: CHT1.4 > CHT3.0 > CHT2.2. Few Lewis acid sites were detected on the surface of MgO. As the desorption temperature increased, the integrated band intensity (i.e., number of pyridine molecules still adsorbed) decreased. At 200 °C, most of the pyridine on CHT1.4–3.0 was desorbed. Higher intensities (> 0.5 a.u.) were only observed for Al_2O_3 and CHT0.6; Al_2O_3 is the only sample to show a band intensity over 0.5 a.u. after evacuation at 300 °C. CHT1.4–3.0 have different amounts of acid sites, but a similar number of stronger acid sites: the amount of weaker acid sites increases from CHT2.2 to CHT3.0 to CHT1.4.

In summary, CHT0.6 has the highest acidity among the CHT samples, with regard number and strength of acid sites; the total amount of acid sites on the other CHT samples is much lower. The acid sites on CHT0.6 and Al_2O_3 are comparable in number, yet the stronger they are, the fewer of them there are on CHT0.6 compared with Al_2O_3. This explains, at least partially, the drastic activity differences between (a) CHT0.6 and Al_2O_3 and (b) CHT0.6 and CHT1.4–3.0.

3.2.1.2. CO_2 adsorption The FTIR spectra (1100–1800 cm^{-1}) of Al_2O_3, MgO, and CHT samples after CO_2 adsorption at 40 °C are shown in Fig. 6. The thermal stability of the surface species was studied by desorption experiments at temperatures up to 300 °C (spectra not shown). Analysis of the spectra permits the detection of surface Brønsted and Lewis base sites and an estimation of their respective amounts and strengths.

3.2.1.3. Surface species The dominant species formed with the surface OH^- groups of Al_2O_3 (Fig. 6a) is bicarbonate (HCO_3^-), with bands at 3609 (ν_{OH}, not shown), 1647 (asym $\nu_{C=O}$), 1476 (sym $\nu_{C=O}$), and 1233 cm^{-1} (δ_{OH}). Surface carbonates are formed to a lesser extent. In the case of surface carbonates, a splitting of the weak asymmetric ν_{CO} vibration (ν_3 mode) (at 1415 cm^{-1} for the free carbonate ion in inorganic salts) is caused by a lowering of the D_{3h} symmetry of the carbonate ion and related to the structure of the surface (adsorbed) carbonate (e.g., monodentate, bidentate, or bridged) [42]. This splitting, $\Delta\nu_3$, generally reflects the strength of the base sites: the lower the splitting, the

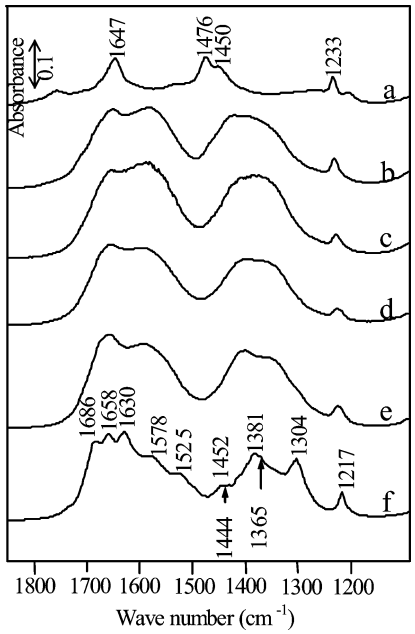

Fig. 6. Base properties: CO_2 adsorption on Al_2O_3 (a), calcined hydrotalcites with Mg/Al ratios of 0.6 (b), 1.4 (c), 2.2 (d), and 3.0 (e), and MgO (f). Spectra were measured after adsorption and evacuation at 40 °C.

stronger the base site. Values measured here are given in the text when applicable. In the case of Al_2O_3, weak bands at 1756 and 1204 cm^{-1} (Fig. 6a) can be assigned to $\nu_{C=O}$ vibrations of bridged "organic-like" complexes on Al_2O_3 and indicate a $\Delta\nu_3$ splitting of 552 cm^{-1} for a weak base site. Weak shoulders at 1704 and 1265 cm^{-1} (not indicated in Fig. 6) can be assigned to bidentate carbonate species ($\Delta\nu_3$ splitting of 439 cm^{-1}) on Al_2O_3. The band at 1450 cm^{-1} may indicate the presence of free carbonate ions.

The spectrum of MgO (Fig. 6f) after CO_2 adsorption is complex, with numerous bands between 1800 and 1100 cm^{-1}. The major bicarbonate species is indicated by the bands at 1630, 1452, and 1217 cm^{-1}. Weaker bands (shoulders) at 1600, 1448, and 1200 cm^{-1} (not indicated in Fig. 6) could belong to a second type of bicarbonate species. Pairs of bands at 1686/1365 cm^{-1} and 1658/1304 cm^{-1} can be assigned to the $\nu_{C=O}$ vibrations of two different bidentate carbonate structures. Based on their low $\Delta\nu_3$ splitting (134 and 144 cm^{-1}, respectively), these bands are normally attributed to monodentate carbonate species [42–44], yet their corresponding high thermal stability (stable up to 300 °C under vacuum, not shown) suggests they are caused by polydentate carbonates [45].

A lower structural variety of carbonates was formed on the surface of CHT samples (Fig. 6b–e). Very broad bicarbonate bands are seen at 1658–1650 cm^{-1} and 1420–1400 cm^{-1}. Based on the $\Delta\nu_3$ splitting (see below), the maxima at 1591–74 cm^{-1} and 1386–65 cm^{-1} can be attributed to monodentate surface carbonates [42–45]. The thermal stability of these species is rather high; their bands are observed even after evacuation at 300 °C. Thus, as in the case of MgO, the polydentate structures formed probably have a structure similar to that of bulk species [42].

3.2.1.4. Strength and amount of base sites According to [44], the formation of different types of carbonates is related to the basicity of the surface oxygen atoms. It was postulated that the structural nonuniformity of surface oxygen ions leads to basicity differences and, thus, causes the formation of different carbonate structures. The spectral parameter, $\Delta\nu_3$, was proposed as a measure of the relative strength of surface base sites [44]: the smaller the $\Delta\nu_3$ value, the stronger the surface basic site that is involved in the interaction with CO_2.

Based on $\Delta\nu_3$, the following can be concluded. Al_2O_3 exhibits the weakest Lewis basicity, with $\Delta\nu_3$ values of 552 and 439 cm^{-1} for the bridged and bidentate carbonate species, respectively. The strongest basicity was observed for MgO, which formed monodentate species with CO_2 and exhibits the smallest $\Delta\nu_3$ of 134 cm^{-1}. The calcined hydrotalcites are less basic than MgO but more basic than Al_2O_3. Here the strength of base sites (decrease in $\Delta\nu_3$) of the CHT samples decreases with increasing Mg content: CHT0.6 (188 cm^{-1}) > CHT1.4 (209 cm^{-1}) > CHT2.2 (225 cm^{-1}) ≈ CHT3.0 (226 cm^{-1}). The relative amount of Lewis base sites was estimated by the integration of the carbonate bands (MgO: 1572, 1444, 1517, 1388 cm^{-1}; CHT: 1574–1581, 1368–1386 cm^{-1}) after evacuation at 150 °C, that is, after removal of bicarbonate species (spectra not shown). When the amount of Lewis base sites was normalized by weight, intensities decreased for the samples in the following order: CHT3.0 ∼ CHT1.4 ∼ MgO > CHT2.2 > CHT0.6 ≫ Al_2O_3. CHT3.0 has the highest number of weak Lewis base sites (higher splitting), whose strengths are similar to those found on CHT2.2; Lewis base sites on CHT0.6, the most catalytically active sample, are the strongest, but few in number. These findings agree with [30], in which the total amount of base sites was increased, but the proportion of stronger base sites decreased with increasing Mg/Al molar ratios.

The intensity of the OH^- deformation band (around 1220 cm^{-1}) for surface bicarbonates after evacuation at 40 °C has been used to quantitatively determine the number of basic OH^- species [43]. Interestingly enough, the decrease in the band intensities (amount of OH^- species) is CHT0.6 > CHT3.0 > CHT1.4 > CHT2.2 (Fig. 7). The shift in the 1220 cm^{-1} band to lower wave number indicates an increase in site strength with Mg content from CHT0.6 to MgO. Thus, CHT0.6 has a high number of Brønsted base sites; CHT3.0 has fewer but stronger sites.

3.2.2. Microcalorimetry

Base sites were additionally characterized by microcalorimetry. The probe molecule, CO_2, was used for gas-phase experiments, a common method; liquid-phase experiments were carried out with benzoic acid in toluene to gain insights into base site behavior under reaction conditions.

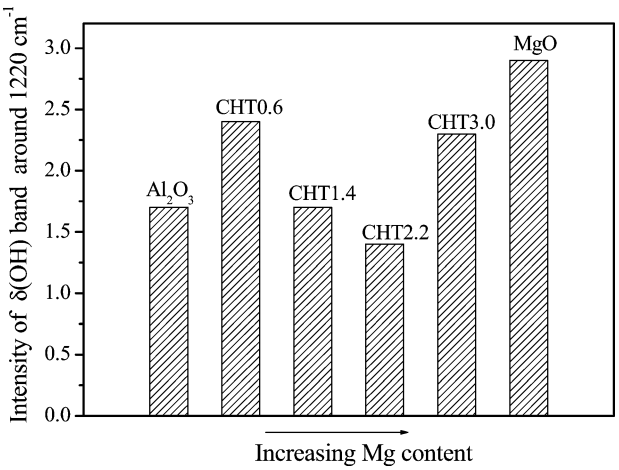

Fig. 7. Base properties: intensity of band around 1220 cm^{-1} after evacuation at 40 °C.

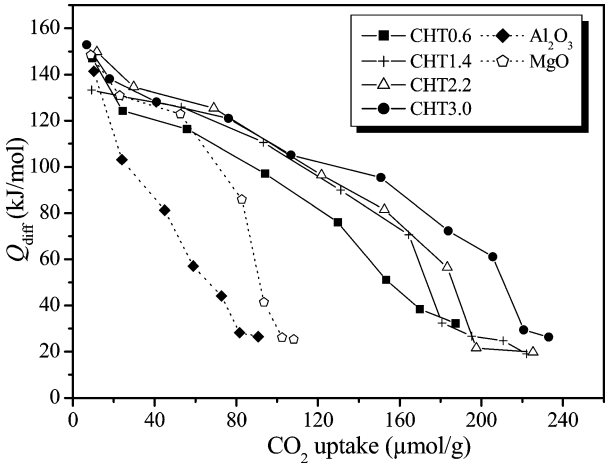

Fig. 8. Base properties: differential heats of CO_2 adsorption at 40 °C as a function of CO_2 uptake.

3.2.2.1. Gas-phase microcalorimetry with CO_2 The differential heats of CO_2 adsorption as a function of CO_2 uptake on calcined hydrotalcites, Al_2O_3, and MgO (Fig. 8) show initial values between 130 and 155 kJ/mol. The CHT samples have more base sites than MgO and Al_2O_3. This applies, in particular, to the increase in the number of weak base sites found on the CHT samples and agrees with the FTIR results. Again, CHT3.0 exhibits the highest number of weak basic sites (compare Section 3.2.1 FTIR studies: CO_2 adsorption). The immediate and continuous decrease in the heats of adsorption with increasing CO_2 uptakes (and the very broad carbonate bands in the FTIR spectra after CO_2 adsorption) indicates a wide distribution of site strength, particularly for the CHT samples. The total uptake of irreversible (chemisorbed) CO_2 decreases in the following order at a differential heat value of 50 kJ/mol: CHT3.0 > CHT1.4 > CHT2.2 > CHT0.6 > MgO > Al_2O_3. With respect to MgO, this order differs somewhat from that observed by CO_2-FTIR. This could be due to the different conditions applied; the microcalorimetric measurements were performed at 40 °C and do not distinguish between Brønsted and Lewis base sites. The FTIR measurements, on the other hand, only characterize Lewis base sites (measurement after evacuation at 150 °C).

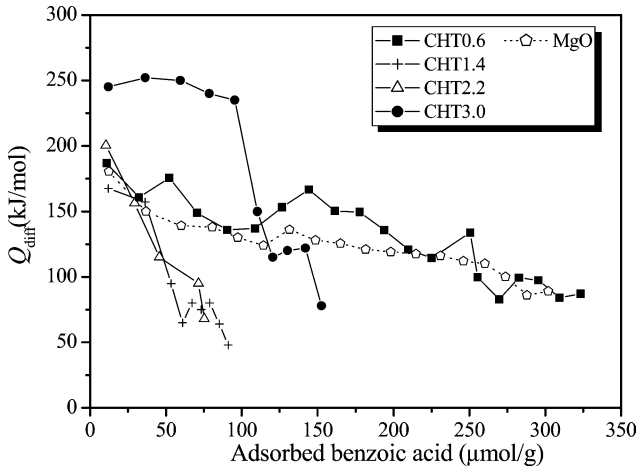

Fig. 9. Base properties: differential heats of adsorption of benzoic acid in toluene measured at 70 °C except for that of MgO (40 °C).

3.2.2.2. Liquid-phase microcalorimetry with benzoic acid Microcalorimetric experiments with a toluene solution of benzoic acid (used to measure the strength and amount of base sites by indicator titration [46]) were performed to characterize basicity under liquid-phase conditions like those of catalytic test reactions. The differential heats of adsorption given in Fig. 9 show a base site behavior that is much different from that found for the experiments with CO_2 (Fig. 8). Here CHT3.0 has much stronger base sites initially, but far fewer than CHT0.6; CHT1.4 and CHT2.2 have even fewer sites, but their strengths are similar to those of CHT0.6. The liquid-phase basicity of MgO is similar to that of CHT0.6, but was measured at a lower experimental temperature of 40 °C (instead of 70 °C); this temperature discrepancy may indicate weaker and fewer base sites in MgO than in CHT0.6.

3.3. Application of the catalysts in Michael additions

3.3.1. Michael addition of 2-methylcyclohexane-1,3-dione to methyl vinyl ketone

The catalyzed Michael addition of 2-methylcyclohexane-1,3-dione ($pK_a = 6.7$) to methyl vinyl ketone yields 2-(3-oxo-butyl)-2-methylcyclohexane-1,3-dione (Scheme 1). The poorly soluble CH-acid compound partially dissolves in methanol to slowly establish a saturation concentration of 0.15 M from a total theoretical concentration of 1.5 M in the reaction mixture; it is then converted into the liquid reaction product. In blank experiments (experiments without a catalyst) with recrystallized 2-methylcyclohexane-1,3-dione, no product formation was observed.

We performed catalytic studies of the HT and CHT samples by monitoring product formation; the activities of the

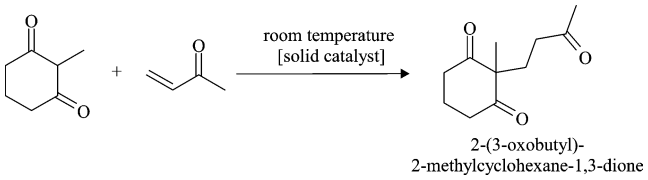

Scheme 1. Michael addition of 2-methylcyclohexane-1,3-dione to methyl vinyl ketone.

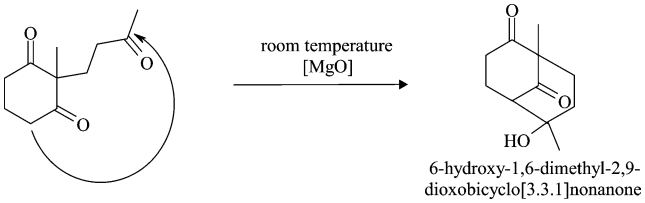

Scheme 2. Consecutive aldol cyclization of the Michael addition product formed according to Scheme 1 on MgO.

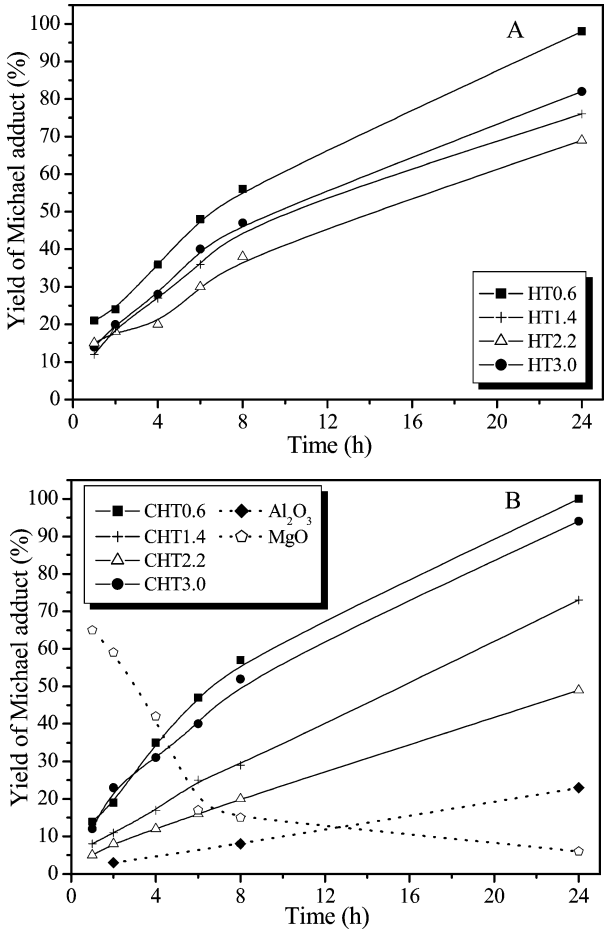

Fig. 10. Results of the Michael addition of 2-methylcyclohexane-1,3-dione (15 mmol) to methyl vinyl ketone (22.5 mmol) in 10 ml methanol according to Scheme 1 over the hydrotalcites (A) and over the calcined hydrotalcites, Al_2O_3 and MgO (B). Catalyst amounts were 0.225 g for the hydrotalcites, Al_2O_3, and MgO and the amount remaining after calcination of 0.225 g hydrotalcite at 550 °C.

solid bases differed significantly (Figs. 10A and 10B, respectively). The target product was formed with 100% selectivity.

The product yields obtained after 24 h on the HT samples decreased in the order HT0.6 > HT3.0 > HT1.4 > HT2.2 and do not correlate with the Mg/Al ratio. Samples with the lowest and highest Mg/Al ratios achieved the highest yields after 24 h: 98% for HT0.6 and 82% for HT3.0 (Fig. 10A).

The catalytic behavior of the CHT samples formed by calcination of the corresponding HT samples (weight loss from dehydration and decarboxylation) remained more or less the same for CHT1.4 and CHT0.6, decreased from 69 to 49% for CHT2.2, and increased from 82 to 94% for CHT3.0 (Fig. 10B). HT2.2 and CHT2.2 exhibited the lowest catalytic activities. The activities of the CHT samples decreased in the same order as the HTs: CHT0.6 > CHT3.0 > CHT1.4 > CHT2.2.

Choudary et al. found that whereas a rehydrated Mg–Al hydrotalcite was an efficient, very selective catalyst for Michael additions, the untreated and calcined hydrotalcites were inactive. This finding was ascribed to their Brønsted base sites. However, the lack of a detailed characterization and discussion of the catalysts tested make a detailed comparison with the results presented here difficult. The differences in the reaction results may be related, however, to the lower acidity of the CH-acid compounds used in [9], compared with the more acidic CH-acid compounds used here.

Regarding the pure oxides, the catalytic activity of Al_2O_3 was lower than that of the CHT samples (Fig. 10B) and may be related to its Lewis acidity or weak basicity or both. Michael additions can be catalyzed by both base and acid catalysts; acid catalysts such as acetic acid [47], a montmorillonite-enwrapped scandium complex [48], or TS-1 molecular sieve [49] have been used before. MgO had a considerably different, less selective behavior than that of the CHT samples or Al_2O_3. In the case of MgO, a high product yield of 65% was formed within the first 30 min, but the amount of the Michael adduct in the reaction mixture dropped drastically during the next 24 h. In the ^{1}H NMR spectra of the reaction mixture, additional CH_3 signals (0.97 and 1.23 ppm) were found for a consecutive product, 6-hydroxy-1,6-dimethyl-2,9-dioxobicyclo[3.3.1]nonane, which was formed by the intramolecular aldol cyclization of 2-methyl-2-(3-oxo-butyl)-cyclohexane-1,3-dione (Scheme 2) and identified with GC-MS.

Catalytic activity decreased in the following order: MgO > CHT0.6 > CHT3.0 > CHT1.4 > CHT2.2 > Al_2O_3. This correlates with the band intensities of the OH^- species (FTIR experiments), except for that of Al_2O_3, which has a band intensity similar to that of CHT1.4 (Fig. 7). The catalytic activities within the CHT sample series also reflect the amounts of base sites detected with liquid-phase microcalorimetry (Fig. 9). The discrepancy between the similar liquid-phase basicities and different catalytic behaviors of CHT0.6 and MgO (Figs. 9 and 10B, respectively) cannot be explained at this time. In gas-phase microcalorimetry,

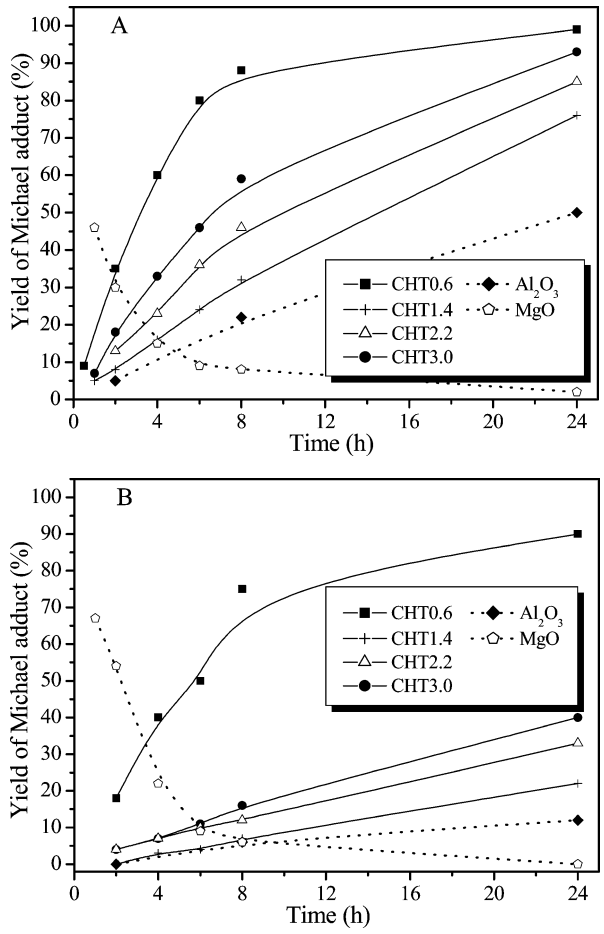

Fig. 11. Results of the Michael additions of 2-acetylcyclopentanone (15 mmol) (A) and 2-acetylcyclohexanone (15 mmol) (B) to methyl vinyl ketone (22.5 mmol) in 10 ml methanol according to Scheme 3 over calcined hydrotalcites (0.225 g).

the CHT samples exhibited basicities, which do not correspond to their catalytic activities in the Michael addition, yet there is a direct relation between Mg contents and the base site interaction with the gaseous probe molecule CO_2 (Fig. 8).

3.3.2. Michael additions of 2-acetylcyclopentanone and 2-acetylcyclohexanone to methyl vinyl ketone

To extend the catalytic application of the CHT samples, further Michael additions were performed with the less acidic CH-acid compounds, 2-acetylcyclopentanone ($pK_a = 7.8$) and 2-acetylcyclohexanone ($pK_a = 10.1$), to give 2-acetyl-2-(3-oxo-butyl)-cyclopentanone and 2-acetyl-2-(3-oxo-butyl)-cyclohexanone, respectively (Scheme 3). In comparison with the solid 2-methylcyclohexane-1,3-dione, these CH-acids are liquids and are completely soluble in methanol. Thus, the catalytic experiments with these compounds are only roughly comparable to those reported in the previous section.

The decreasing order of catalytic activity was identical for the addition of both 2-acetylcyclopentanone and 2-acetylcyclohexanone (Figs. 11A and 11B, respectively): MgO > CHT0.6 > CHT3.0 > CHT2.2 > CHT1.4 > Al_2O_3.

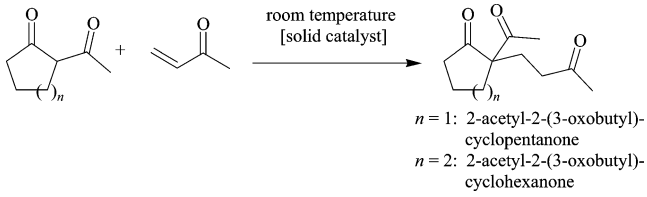

Scheme 3. Michael addition of 2-acetylcyclopentanone ($n = 1$) and 2-acetylcyclohexanone ($n = 2$) to methyl vinyl ketone.

The Michael addition of 2-acetylcyclopentanone to methyl vinyl ketone proceeded faster than that of 2-acetylcyclohexanone, except in the case of MgO. This can be explained by the higher acidity and more favored deprotonation of 2-acetylcyclopentanone by the base sites. Consequently, the carbanion formed as the reactive species is present in higher equilibrium concentration.

CHT0.6 exhibited an outstanding catalytic activity in the Michael addition reaction of the less acidic CH-acid compound, 2-acetylcyclohexanone (Fig. 11B; compare with Fig. 11A). The activities of the other CHT samples and Al_2O_3 are significantly lower. Their basicities may be too weak to sufficiently deprotonate the CH-acid compound, yet the amount of Lewis base sites determined does not completely explain the performance of CHT0.6. Acid sites may also facilitate the catalytic process; Al_2O_3 shows a considerable activity in the Michael addition of 2-acetylcyclopentanone ($pK_a = 7.8$) (Fig. 11A). The mild acid sites on Al_2O_3 and the presence of weak base sites catalyze the addition with more reactive diones to some extent, and the active sites determining catalytic activity are, in fact, the base sites.

MgO, on the other hand, showed a similar catalytic behavior in the experiments with 2-acetylcyclopentanone and 2-acetylcyclohexanone and the reaction of 2-methylcyclohexane-1,3-dione. Products formed rapidly initially, with final catalytic yields drastically decreasing thereafter (cf. Figs. 11A and 11B).

A similar relationship exists between catalyst activity and basicity (characterized by liquid-phase microcalorimetry and the OH^- band intensity at 1220 cm^{-1}) for all three Michael additions. The only exception is the inversed catalytic activity of CHT1.4 and CHT2.2.

Solvent-free reactions with the most active samples, CHT0.6 and CHT3.0, examined the environmentally friendly implementation of the Michael additions (Scheme 3). CHT0.6 attained the highest activities; nevertheless, yields of the target products were lower than those found when a solvent was used for both catalysts after 24 h. The decrease in yields for the solvent-free reaction with 2-acetylcyclopentanone is much more drastic (Fig. 12A) than for that with 2-acetylcyclohexanone (Fig. 12B). The low (delayed) product formation may be related to the absence of carbanion stabilization by methanol. Nonetheless, the inves-

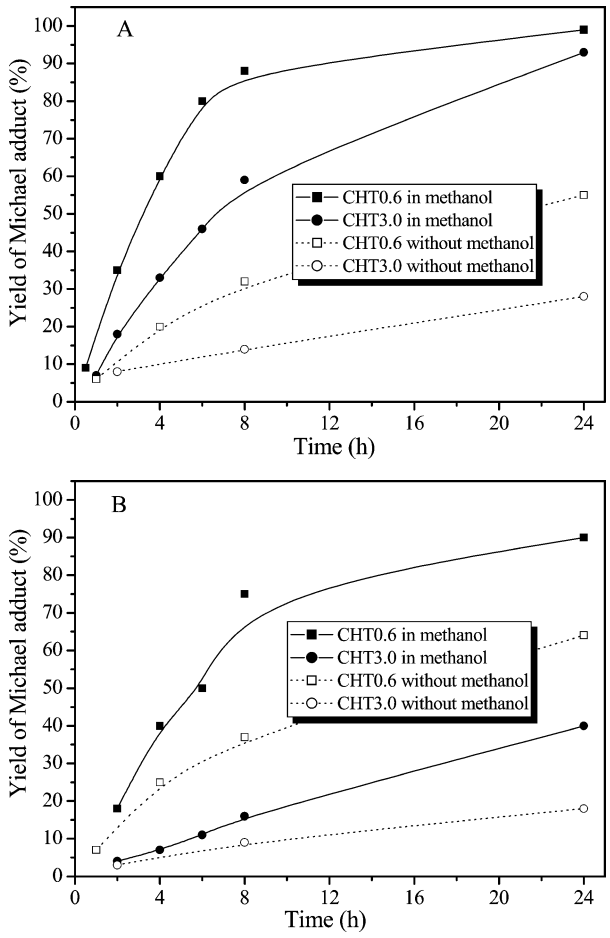

Fig. 12. Results of the solvent-free Michael additions of 2-acetylcyclopentanone (15 mmol) (A) and 2-acetylcyclohexanone (15 mmol) (B) to methyl vinyl ketone (22.5 mmol) on CHT0.6 and CHT3.0 (0.225 g).

tigated Michael additions can be performed under solvent-free conditions, but with longer reaction times.

3.3.3. Investigations of the type of catalysis

Experiments on the type of catalysis (homogeneous or heterogeneous) involved in the Michael additions showed that although the product yield continued to increase after removal of the solid catalyst (CHT0.6) in the presence and absence of methanol, the reactions proceed considerably more slowly than they do without catalyst separation (via centrifugation). Final yields (20 h after catalyst separation) increased from 49 to 76% and from 35 to 70% in the reactions with cyclohexane-1,3-dione (Experiment A) and 2-acetyl-cyclohexanone (Experiment B) in methanol. The solvent-free reaction with 2-acetylpentanone (Experiment C) had a corresponding yield of 34% up from 21% (20 h after the catalyst was separated). The titrated reaction solution of Experiment B had a Mg content of about 4% of the total Mg content in the catalyst, and 0.3% of the Al cations in the catalyst were found in this solution. However, because the catalyst is a very fine powder, instead of being completely separated, some of the solid catalyst may still be finely dispersed in the reaction solution. In addition, the presence of EDTA, a good complexing agent for Mg (pK_B for Mg-EDTA complex: 8.65 [50]), allows a better dissolution of the Mg cations than that of the Al cations (pK_B for Al-EDTA complex: 16.7 [50]) during titration; this explains the much higher Mg content found. Thus, the increase in yield after catalyst separation is most likely caused by fine particles of the solid catalyst still in the solution (heterogeneous catalysis) and not homogeneous catalysis.

The liquid-phase basicity microcalorimetry measurements with benzoic acid in toluene correlated very well with the reaction results, yet benzoic acid is not able to form a chelate with Mg, and Mg is unlikely to leach in toluene. Thus, leaching can be excluded from these measurements. Based on this and the low Mg content in the solution after a questionable separation of the catalyst, we conclude that homogeneous catalysis plays a very minor role, if any, in the catalytic reactions studied here.

4. Conclusions

- The calcined hydrotalcites (periclase MgO stucture) exhibit Lewis acid, Brønsted base, and Lewis base sites. The calcined Al-rich sample (Mg/Al molar ratio of 0.6, amorphous MgO) possesses Lewis acid sites similar in strength to those found on Al_2O_3, but stronger than those found on the Mg-rich hydrotalcites.
- Both the uncalcined hydrotalcites and the calcined hydrotalcites catalyze the Michael additions of 2-methylcyclohexane-1,3-dione, 2-acetylcyclopentanone, and 2-acetylcyclohexanone to methyl vinyl ketone with high selectivity (no side product formation). These Michael additions in methanol proceeded faster than the solvent-free reactions. Experiments on the type of catalysis involved indicated that homogeneous catalysis is less probable, but could not be totally disregarded.
- Pure Al_2O_3 was the least active among the investigated catalysts. Both the Al-rich hydrotalcite with traces of boehmit and the calcined Al-rich sample (Mg/Al molar ratio of 0.6) gave product yields above 95% within 24 h.
- A nonlinear correlation between the Mg content and catalytic activity suggested that the activity of pure MgO surpasses that of the calcined hydrotalcites but causes consecutive reactions of the Michael addition products, which reduce the product selectivities and yields.
- Catalytic activity correlates with the amount of the base sites determined by benzoic acid microcalorimetry dependent on the Mg/Al molar ratio.
- An optimal balance of acid–base properties may make the calcined Al-rich hydrotalcite an excellent catalyst in the Michael addition of numerous 1,3-diones independently of their pK_a values.

Acknowledgments

We acknowledge the Bundesministerium für Bildung und Forschung (FKZ 03C0328) for their financial support. We also thank Dr. M. Feist for the thermal analysis, W. Ziesche for adsorption experiments, Dr. J. Radnik for XPS measurements, and Dr. D. Heidemann for MAS NMR measurements.

References

[1] H. Hattori, Stud. Surf. Sci. Catal. 78 (1993) 35.
[2] H. Hattori, Chem. Rev. 95 (1995) 537.
[3] J. Barrios, R. Rojas, A.R. Alcanrara, J.V. Sinisterra, J. Catal. 112 (1988) 528.
[4] H. Kabashima, H. Tsuji, H. Hattori, Appl. Catal. A 165 (1997) 319.
[5] H. Kabashima, H. Tsuji, T. Shibuya, H. Hattori, J. Mol. Catal. A 155 (2000) 23.
[6] H. Kabashima, H. Tsuji, S. Nakata, H. Hattori, Appl. Catal. A 194–195 (2000) 227.
[7] U. Meyer, H. Gorzawski, W.F. Hölderich, Catal. Lett. 59 (1999) 201.
[8] Z.-J. Li, H.A. Prescott, J. Deutsch, A. Trunschke, H. Lieske, E. Kemnitz, Catal. Lett. 92 (2004) 175.
[9] B.M. Choudary, M.L. Kantam, Ch.V. Reddy, K.K. Rao, F. Figueras, J. Mol. Catal. A 146 (1999) 279.
[10] M.J. Climent, A. Corma, S. Iborra, J. Primo, J. Catal. 151 (1995) 60.
[11] A. Corma, V. Fornés, R.M. Martin-Aranda, F. Rey, J. Catal. 134 (1992) 58.
[12] F. Cavani, F. Trifiro, A. Vaccari, Catal. Today 11 (1991) 173.
[13] A. Vaccari, Catal. Today 41 (1998) 53.
[14] B.F. Sels, D.E. De Vos, P.A. Jacobs, Catal. Rev. Sci. Eng. 43 (2001) 443.
[15] D. Tichit, B. Coq, CATTECH 7 (2003) 206.
[16] A.L. McKenzie, C.T. Fishel, R.J. Davis, J. Catal. 138 (1992) 547.
[17] J.I. Di Cosimo, V.K. Díez, M. Xu, E. Iglesia, C.R. Apesteguía, J. Catal. 178 (1998) 499.
[18] J. Shen, J.M. Kobe, Y. Chen, J.A. Dumesic, Langmuir 10 (1994) 3902.
[19] V.K. Díez, C.R. Apesteguía, J.I. Di Cosimo, J. Catal. 215 (2003) 220.
[20] F. Prinetto, G. Ghiotti, R. Durand, D. Tichit, J. Phys. Chem. B 104 (2000) 11117.
[21] J. Shen, M. Tu, C. Hu, J. Solid State Chem. 137 (1998) 295.
[22] S. Casenave, H. Martinez, C. Guimon, A. Auroux, V. Hulea, A. Cordoneanu, E. Dumitriu, Thermochim. Acta 379 (2001) 85.
[23] S. Casenave, H. Martinez, C. Guimon, A. Auroux, V. Hulea, E. Dumitriu, J. Therm. Anal. Cal. 72 (2003) 191.
[24] P.S. Kumbhar, J.S. Valente, J. Lopez, F. Figueras, Chem. Commun. (1998) 535.
[25] K. Yamaguchi, K. Ebitani, T. Yoshida, H. Yoshida, K. Kaneda, J. Am. Chem. Soc. 121 (1999) 4526.
[26] D. Tichit, D. Lutic, B. Coq, R. Durand, R. Teissier, J. Catal. 219 (2003) 167.
[27] D. Tichit, M.H. Lhouty, A. Guida, B.H. Chiche, F. Figueras, A. Auroux, D. Bartalini, E. Garrone, J. Catal. 151 (1995) 50.
[28] M.J. Climent, A. Corma, S. Iborra, K. Epping, A. Velty, J. Catal. 225 (2004) 316.
[29] www.sasol.com, product information.
[30] A. Corma, V. Fornés, F. Rey, J. Catal. 148 (1994) 205.
[31] G. Fornasari, M. Gazzano, D. Matteuzi, F. Trifiro, A. Vaccari, Appl. Clay Sci. 10 (1995) 69.
[32] K.J.D. MacKenzie, R.H. Meinhold, B.L. Sherriff, Z. Xu, J. Mater. Chem. 3 (1993) 1263.
[33] W.T. Reichle, S.Y. Kang, D.S. Everhardt, J. Catal. 101 (1986) 352.
[34] S. Miyata, Clays Clay Miner. 28 (1980) 50.
[35] H. Knözinger, Adv. Catal. 25 (1976) 184.
[36] G. Busca, Phys. Chem. Chem. Phys. 1 (1999) 723.
[37] N. Fripiat, R. Conanec, A. Auroux, Y. Laurent, P. Grange, J. Catal. 167 (1997) 543.
[38] C. Morterra, A. Chiorino, G. Ghiotti, E. Garrone, J. Chem. Soc., Faraday Trans. 1 75 (1979) 271.
[39] C. Morterra, S. Coluccia, A. Chiorino, F. Boccuzzi, J. Catal. 54 (1978) 348.
[40] F. Abbattista, S. Delmastro, G. Gozzelino, D. Mazza, M. Vallino, G. Busca, V. Lorenzelli, G. Ramis, J. Catal. 117 (1989) 42.
[41] P. Nortier, P. Fourre, A.B. Mohammed Saad, O. Saur, J.C. Lavalley, Appl. Catal. 61 (1990) 141.
[42] J.C. Lavalley, Catal. Today 27 (1996) 377.
[43] J.A. Lercher, C. Colombier, H. Noller, J. Chem. Soc., Faraday Trans. 1 80 (1984) 949.
[44] A.A. Davydov, M.L. Shepot'ko, A.A. Budneva, Kinet. Catal. 35 (1994) 299.
[45] G. Busca, V. Lorenzelli, Mater. Chem. 7 (1982) 89.
[46] K. Tanabe, M. Misono, Y. Ono, H. Hattori, New Solid Acids and Bases—Their Catalytic Properties, Stud. Surf. Sci. Catal., vol. 51, Elsevier, Tokyo, 1989, p. 14.
[47] T. Bui, C.F. Barbas, Tetrahedron Lett. 41 (2000) 6951.
[48] T. Kawabata, T. Mizugaki, K. Ebitani, K. Kaneda, J. Am. Chem. Soc. 125 (2003) 10486.
[49] M. Sasidharan, R. Kumar, J. Catal. 220 (2003) 326.
[50] N. Wiberg (Ed.), Lehrbuch der Anorganischen Chemie, hundred first ed., Walter de Gruyter, Berlin, 1995, p. 1219.